Journal of Magnetism and Magnetic Materials 401 (2016) 1078–1087

Contents lists available at ScienceDirect

Journal of Magnetism and Magnetic Materials

journal homepage: www.elsevier.com/locate/jmmm

Current Perspectives

Control of flow around a circular cylinder wrapped with a porous layer by magnetohydrodynamic

M. Bovand [a], S. Rashidi [b], J.A. Esfahani [b,*], S.C. Saha [c], Y.T. Gu [c], M. Dehesht [d]

[a] Department of Mechanical Engineering, Semnan Branch, Islamic Azad University, Semnan, Iran
[b] Department of Mechanical Engineering, Ferdowsi University of Mashhad, Mashhad 91775-1111, Iran
[c] School of Chemistry, Physics and Mechanical Engineering, Queensland University of Technology, GPO Box 2434, Brisbane, QLD 4001, Australia
[d] School of Mechanical Engineering, Semnan University, P.O. Box 35196-45399, Semnan, Iran

ARTICLE INFO

Article history:
Received 30 June 2015
Received in revised form
2 November 2015
Accepted 4 November 2015
Available online 11 November 2015

Keywords:
Magnetohydrodynamic
Porous medium
Stuart number
Laminar flow
Vortex shedding
Lorentz force

ABSTRACT

The present study focuses on the analysis of two-dimensional Magnetohydrodynamic (MHD) flow past a circular cylinder wrapped with a porous layer in different laminar flow regimes. The Darcy-Brinkman-Forchheimer model has been used for simulating flow in porous medium using finite volume based software, Fluent 6.3. In order to analyze the MHD flow, the mean and instantaneous drag and lift coefficients and stream patterns are computed to elucidate the role of Stuart number, N and Darcy number, Da. It is revealed that the magnetic fields are capable to stabilize flow and suppress the vortex shedding of vortices. The N-Re plane shows the curves for separating steady and periodic flow regimes, N_{cr} and disappearing of vortex, N_{diss}. For validate the solution, the obtained C_D and St are compared with available results of literature.

1. Introduction

Fluid flow around one or more cylinders in absence of magnetic field has been extensively studied for several decades with a wide range of experimental [1–4] and numerical [5–9] methods. It is reported that the flow around a circular cylinder in absence of magnetic field is steady for the range of Reynolds number $0 < Re \leq 46$. However, for $Re \geq 46$ the flow becomes unstable such that vortices shed periodically.

The study of magnetohydrodynamic (MHD) flow has received considerable attention because of its application in industrial and engineering such as stirring, pumping, crystal growth process and cooling circuits of fast fission reactors [10–14]. Many efforts to investigate MHD flows have been made in the past, based on theoretical, numerical and experimental analysis. In 1832, Michael Faraday set up a magnetohydrodynamic power generator with two copper electrodes and placed them in the river Thames in London and measured a voltage between them. After that, many investigators studied MHD flows for different configurations. The study of streamwise magnetic fields is considered in [15,16] experimentally and in [17–22] numerically. Also good results for transverse magnetic field can be found in [23,24] (experiments) and in [17,18,20] (numeric).

Yoon et al. [19] found when the uniform magnetic fields aligned with the free stream are applied to the flow past a circular cylinder, the Lorentz force acting on the flow damps the flow oscillation caused by the vortex shedding. They established the critical value for Stuart number N_{cr} (Stuart number "N" is the ratio of electromagnetic force to inertia force), which makes the time-dependent fluid flow and temperature fields steady, depends on Reynolds number. As the intensity of magnetic fields increases, the vortex shedding formed in the wake becomes weaker and the oscillating amplitude of lift coefficient decreases. The authors found pressure drag coefficient (C_{DP}) and drag coefficient (C_D) decrease slightly with increasing of N when $N < N_{cr}$. Grigoridis et al. [20] proposed an extension of the immersed boundary (IB) method that accounts for electromagnetic effects near non-conducting boundaries in MHD flows. They called it MIB method. They investigated the performance of MIB method and demonstrated its potential for the computation of MHD flows in complex geometries. They studied the flow of a conducting fluid past a circular cylinder under streamwise and transverse magnetic fields. In the steady flow regime, the value of drag coefficient was found to vary according to $(N_x+c)^{1/2}$ and the recirculation length according to e^{-cNx} where N_x is interaction parameter for streamwise magnetic field and c is constant parameter. Hussam et al. [25] investigated the dynamics and heat transfer characteristics of a quasi-two-dimensional MHD flow past a confined circular cylinder with a

* Corresponding author.
E-mail address: abolfazl@um.ac.ir (J.A. Esfahani).

http://dx.doi.org/10.1016/j.jmmm.2015.11.019
0304-8853/

Nomenclature

B	Magnetic field strength (T), $B=B_0R/r$
B_0	Constant magnetic field at surface of cylinder (T)
C	A dimensionless coefficient (dimensionless)
d	Thickness of porous layer (m)
D	Diameter (m)
Da	Darcy number (dimensionless), $Da=K/D^2$
F	Force (N)
f	Wake oscillation frequency(s^{-1})
J	Electrical current density (A/m^2)
K	Permeability (m^2)
N	Stuart number (dimensionless), $N=\sigma B^2D/(\rho U_\infty)$
p	Pressure (Pa)
r	Radial coordinate (m)
R	Cylinder radius (m),$R=D/2$
Re	Reynolds number (dimensionless), $\rho U_\infty D/\mu$
St	Strouhal number (dimensionless), $=f\ D/U_\infty$
t	Time (s)
u	Velocity vector (ms^{-1})
U	Velocity (ms^{-1})

Greek symbols

μ	Dynamic viscosity $(kg\,m^{-1}\,s^{-1})$
υ	Fluid kinematic viscosity $(m^2\,s^{-1})$, $\upsilon=\mu/\rho$
ρ	Fluid density $(kg\,m^{-3})$
ε	Porosity (dimensionless)
θ	Cross-radial coordinate (dimensionless)
σ	Electrical conductivity of the fluid $(1/\Omega m)$
ω	Vorticity $(1/s)$

Subscripts/superscripts

ave	Average
c	particle
cr	Critical
d,D	Drag
diss	Disappearance
f	Fluid
F	Forchheimer
L	Lift
p	Pressure
R	Recirculating
s	Solid
v	Viscous
ω	Vorticity $(1/s)$
∞	Free stream
1	Clear fluid domain
2	Porous domain
$+$	Porous-wrapped solid cylinder

strong magnetic field for Reynolds number $50<\mathrm{Re}<3000$, Hartman number (the ratio of electromagnetic force to the viscous force) $0<\mathrm{Ha}<1200$, and blockage ratio $0.1<\beta<0.4$. They used rectangular duct confining a circular cylinder placed at the centre of the duct parallel to the transverse direction and perpendicular to the flow direction. One of the walls oriented parallel to the magnetic field is heated to a constant wall temperature Tw whereas the other surfaces are thermally insulated. Their results revealed that the heat transfer rate (from the wall) is strongly dependent on the Hartmann number, and that the pressure loss (the difference in pressure drop across identical channels with and without a circular cylinder generated by adding a cylinder to the channel) increases with the Hartmann number and found transition from steady to unsteady flow regimes that is determined as a function of Hartmann number and blockage ratio.

Several studies have also been undertaken to study purely hydrodynamic flows in porous media [26,27]. Bruneau and Mortazavi [28–31] investigated the passive control of vortex shedding from a cylinder using a porous sheath. The presence of the porous layer decreases the shear effects in the boundary layer and improves the vortex shedding, reducing the wake instabilities and the damaging effects of the vortex induced vibrations on the body. Sobera et al. [32] investigated flow at subcritical $\mathrm{Re}=3900$ around a circular cylinder, surrounded at some fixed small distance by a porous layer with a hydraulic resistance typical for that of textile materials. Yu et al. [33] investigated flow past and through a porous square cylinder. They found recirculating wake existing downstream of the cylinder is completely detached from the body under a certain range of parameters. Rashidi et al. [34] simulated the fluid flow and forced convection heat transfer around and through a square diamond-shaped porous cylinder. In their study, Reynolds and Darcy numbers are varied within the ranges of $1<\mathrm{Re}<45$ and $10^{-6}<\mathrm{Da}<10^{-2}$ respectively. The porosity (ε) is 0.5. They found that the drag coefficient decreases and flow separation from the cylinder is delayed with increasing Darcy number. Valipour et al. [35] investigated flow around and through a porous diamond-square cylinder numerically. Their numerical results indicate that the wake length and pressure coefficient decrease when Darcy number increases. Some researchers investigated the effects of magnetic field on fluid flow and heat transfer inside a porous medium. For example, Abd-Alla et al. [36] studied the effects of both rotation and an external magnetic field on peristaltic flow inside a porous medium. It was found that the spin velocity decreases with an increase in Hartmann number. Jiang et al. [37] investigated the effects of a magnetic field on thermomagnetic convection of air inside a porous square enclosure. They observed two vortexes with different intensities and rotational directions inside the porous enclosure at higher values of magnetic force. Ramesh and Devakar [38] investigated the effects of magnetic field on the flow through the porous medium inside an inclined asymmetric channel. Their results indicated that the best pumping rate is occurred at higher values of the magnetic field. Valipour et al. [39] performed a study on Magnetohydrodynamics flow and heat transfer around a solid circular cylinder wrapped with a porous layer. They applied the least square method [40-42] to suggest empirical equations for average Nusselt number. Note that the effect of Darcy numbers and magnetic field are taken into account.

In the literature, three cases of streamwise, transverse, and spanwise magnetic field have been studied. However, very few papers were published related to the effect of magnetic field, created by electric current passed through the wire. This paper presents the results of an extensive numerical study of flow around porous-wrapped circular cylinder (wire) in the presence of the magnetic field of current. The effect of magnetic field (magnetic field around current-carrying wire) on several hydrodynamics parameters, such as the drag coefficient, lift coefficient and the streamlines in the laminar flow regime have been investigated in this literature.

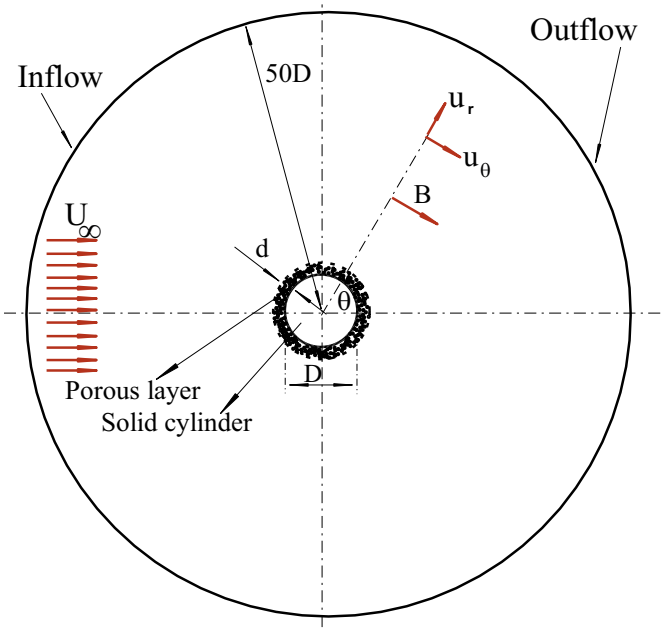

Fig. 1. Schematic diagram of the computational set-up.

2. Numerical analysis

2.1. Problem statement

The system of interest is a two-dimensional circular cylinder with diameter "*D*" wrapped with a porous layer with thickness "$d=0.5$ R". Incompressible fluid of density ρ, molecular viscosity μ and electrical conductivity σ is considered. Far from the cylinder, the flow is unidirectional and uniform. Flow with upstream velocity U_∞ flows around a circular cylinder wrapped with porous layer (Fig. 1). In this study following assumptions were made:

- The fluid is considered to be continuum and conductor of electricity.
- The cylinder is very long such that the flow is invariant along the spanwise direction.
- The fluid flow is unsteady and it limits to the cases of incompressible flow of constant transport property.
- Polarization currents are ignored.
- The porous medium is considered to be rigid, homogeneous and isentropic and saturated with the same single-phase as that in the homogeneous fluid.
- The direction of the magnetic field around current-carrying wire is given by the right-hand rule so, the magnetic field source is placed at the center of cylinder and it is assumed that B_0 is the magnetic intensity at surface of cylinder and B varies as $1/r$ ($\vec{B} = B_0\frac{R}{r}\hat{e}_\theta$). Note that for long cylinder the second assumption is consistent.
- The layer of porous around solid cylinder is larger than the characteristic radius of the medium's pores and satisfied the volume-averaging equations used in this study [43].

2.2. Governing equations

The flows in the homogeneous fluid region and in the porous region are governed by Navier-Stokes equations and Darcy-Brinkman-Forchhiemer extended equation. The governing equations are divided into two zones, the clear fluid zone and the porous medium zone [44]; hence two sets of equations were considered here. A set for clear domain, which are indicated by subscribe Eq. (1), and another set for porous medium, which are denoted by subscribe Eq. (2).

Governing equations for the clear fluid domain are as follows:

2.2.1. Governing equations for the clear domain

Mass conservation equation:

$$\nabla.\ \vec{u_1} = 0 \tag{1}$$

Momentum equation [45]:

$$\rho\frac{\partial\vec{u_1}}{\partial t} + \rho\vec{u_1}.\ \nabla\vec{u_1} = -\nabla.\ P + \mu\nabla^2\vec{u_1} + \underbrace{(\vec{J}\times\vec{B})}_{\text{LorentzForce}} \tag{2}$$

Where $(\vec{J}\times\vec{B})$ is the Lorentz force.

2.2.2. Governing equations for porous zone

Mass conservation equation:

$$\nabla.\ \vec{u_2} = 0 \tag{3}$$

Momentum equation:

$$\frac{\rho}{\varepsilon}\frac{\partial\vec{u_2}}{\partial t} + \rho\frac{\vec{u_2}}{\varepsilon}.\ \nabla\frac{\vec{u_2}}{\varepsilon} = -\nabla.\ P - \underbrace{\frac{\mu}{K}\vec{u_2}}_{\text{DarcyTerm}} + \underbrace{\frac{\mu}{\varepsilon}\nabla^2\vec{u_2}}_{\text{BrinkmanTerm}} - \underbrace{\frac{\rho C_F\left|\vec{u_2}\right|}{\sqrt{K}}\vec{u_2}}_{\text{ForchheimerTerm}} \tag{4}$$

Where Da and Re are the Darcy number and the Reynolds number respectively and are defined by:

$$Da = \frac{K}{D^2},\ \mathrm{Re} = \frac{\rho U_\infty D}{\mu} \tag{5}$$

Note that the local average velocity and intrinsic average velocity can be linked by the Dupuit-Forchheimer relationship [46,47] as $u=\varepsilon U$.

Where U is an averaged velocity over the volume occupied by the fluid phase.

2.3. Governing parameters

Stuart number or interaction parameter, N, which is the ratio of electromagnetic force to inertia force and expressed as [19,48]:

$$N = \frac{\sigma {B_0}^2 D}{\rho U_\infty} \tag{6}$$

The Forchheimer coefficient, C_F, is defined by [33]:

$$C_F = \frac{1.75}{\sqrt{150\varepsilon^3}} \tag{7}$$

The porosity (ε) and Darcy number (Da) could be related through the Carman–Kozeny relation given by [33,39,46,49]:

$$K = \frac{1}{150}\frac{\varepsilon^3 D_c^2}{(1-\varepsilon)^2} \tag{8}$$

Where K is the permeability and D_c is the characteristic diameter of a particle in the permeable medium, each of which may be of 100 μm in diameter.

Drag coefficient is defined as follows [50,51]:

$$C_D = C_{D_v} + C_{D_p} = \frac{F_d}{\frac{1}{2}\rho U_\infty^2 D} \tag{9}$$

Here, subscripts "p" and "v" denotes the pressure and viscous forces, respectively. The drag force per unit length on the cylinder is calculated as [7]:

$$F_d = \frac{DU_\infty}{2}\int_0^{2\pi}(-p\rho U_\infty \cos\theta - 2u\omega \sin\theta)d\theta \tag{10}$$

The wake oscillation frequency "f" is parameterized by Strouhal number:

$$St = \frac{fD}{U_\infty} \tag{11}$$

2.4. Boundary conditions

To minimize the effect of outer boundaries, the radius of the computational domain is defined as 50 times of the cylinder diameter (Fig. 1). The governing Eqs. (1)–(4) are subjected to the following boundary conditions:

On the surface of the solid cylinder ($r=1$):

$$u_2 = 0 \tag{12}$$

Along the upstream boundary (uniform flow):

$$\text{for}\frac{\pi}{2} < \theta < \frac{3\pi}{2} \Rightarrow u_{r1} = \cos\theta,\ u_{\theta 1} = -\sin\theta \tag{13}$$

Along the downstream boundary:

$$\text{for} -\frac{\pi}{2} < \theta < \frac{\pi}{2} \Rightarrow \frac{\partial u_{r1}}{\partial r} = 0,\ \frac{\partial u_{\theta 1}}{\partial r} = 0 \tag{14}$$

Region in which the porosity varies rapidly are generally associated with the boundary between a porous medium and either a homogeneous fluid or a homogeneous solid. Those regions can be conveniently treated in terms of momentum jump condition [52,53]. For this purpose the stress jump condition OTW (Ochoa-Tapia and Whitaker) [54,55] is applied at the porous-fluid interface:

$$\underbrace{\frac{\mu}{\varepsilon}\frac{\partial u_{\theta 2}}{\partial n}}_{\text{Porous}} - \underbrace{\mu\frac{\partial u_{\theta 1}}{\partial n}}_{\text{fluid}} = \underbrace{\beta_1\frac{\mu}{\sqrt{K}}u_\theta}_{\text{interface}} + \beta_2\rho u_\theta^2 \tag{15}$$

In which β_1 and β_2 are adjustable parameters that both are order 1 [55,56] and $u_{\ominus 2}$ and $u_{\ominus 1}$ are the Darcy velocity component parallel to the interface and fluid velocity component parallel to the interface respectively. The continuity of velocity and normal stress prevailing at the interface is given by [33]:

$$\vec{u}_1 = \vec{u}_2 \tag{16}$$

$$\frac{\mu}{\varepsilon}\frac{\partial u_{r2}}{\partial n} - \mu\frac{\partial u_{r1}}{\partial n} = 0 \tag{17}$$

In which u_{r2} and u_{r1} are the Darcy velocity component normal to the interface and fluid velocity component normal to the interface respectively [33].

3. Numerical methodology

In the present computation, governing Eqs. (1)–(4) with the relevant boundary conditions are to be solved numerically by using Finite-Volume based software Fluent 6.3. "Pressure-based solver" has been used to solve governing equation sequentially [57].

Staggered grid system is used where the velocity component are stored at cell faces while pressure and temperature are stored at cell center. The SIMPLE algorithm is utilized for pressure-velocity de-coupling and iteration [58]. The discretization of the governing equation is accomplished by means of second-order upwind (SOU). The first order upwind scheme has been used for discretization of the MHD term in governing equation.

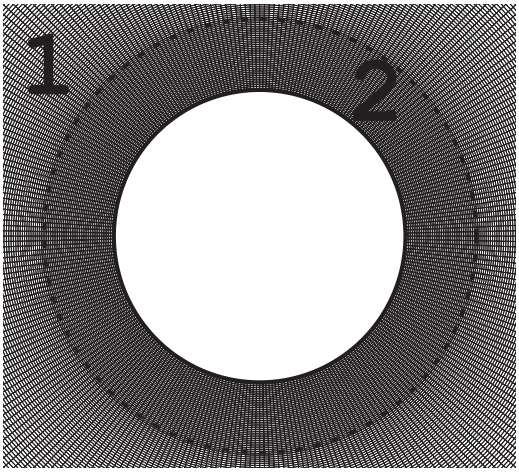

Fig. 2. Mesh distribution in the computational domain near the cylinder.

Lower under-relaxation factors ranging from 0.2 to 0.3 are chosen. For convergence, the summation of residuals are assumed to be $<10^{-6}$ for all equations. The numerical simulation was used to find the hydrodynamics of the flow, velocity distribution; then other parameters such as drag coefficient and streamlines were determined.

4. Grid independence study

Fig. 2 shows a non-uniform and uniform grid distribution along the r- and θ-directions near the cylinder. The whole computational domain was divided into two sub-domains, 1 and 2 for clear and porous domain respectively. The grid in the radial direction were stretched with dense grid in r-direction with $\delta r=0.003$. To ensure a grid-independent solution, the problem is tested for different grid sizes for both solid cylinder and porous-wrapped solid cylinder. The results of this test are available at Rashidi et al. [44] and Valipour et al. [39]. Finally, a suitable grid size was chosen for the final solution.

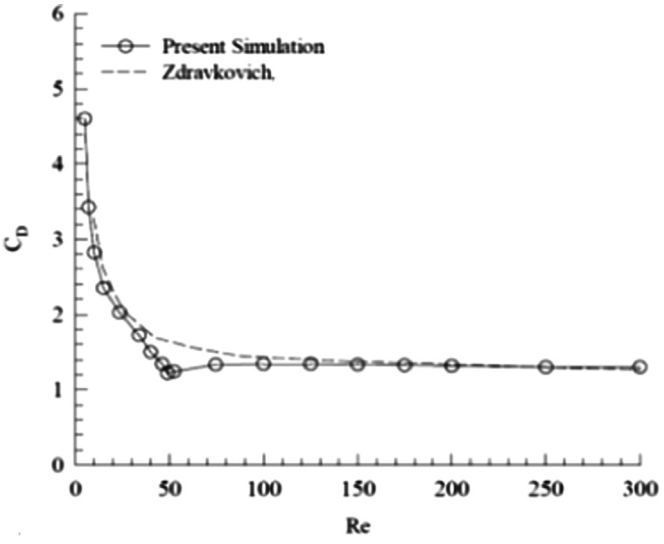

Fig. 3. Drag coefficient (C_D) as a function of Reynolds numbers for flow through a solid circular cylinder.

5. Validation

Validation was performed against published results to ensure the accuracy of the present formulation. Fig. 3 shows the variation of Drag coefficient with Reynolds number together with [52] results and have good agreement. Also, more validations are available at Rashidi et al. [44] and Valipour et al. [39].

6. Results and discussion

In the present study, the following values for the flow parameters are considered:

Reynolds number: Re = 0–400, Darcy number: Da = 10^{-6}–10^{-2}, Stuart number: N = 0–10

6.1. For solid cylinder

In absence of magnetic field, Fig. 3 shows the drag coefficient (C_D) as the function of Reynolds number in the range $0 < Re < 400$. The comparison against the results of Ref. [52] shows an excellent agreement. It is obtained that drag coefficient (C_D) is 1.34 at Re = 100. There are large number of literature exists where the researchers applied streamwise or transverse magnetic fields [17–21].

For 2-D flow along x–y plane (refer Fig. 1), the Lorentz forces f_r and f_θ acting on the fluid is defined as:

Streamwise field:

$$F_r = N(u_{r1}(\sin\theta)^2 + u_{\theta 1}(\mathrm{Sin}\,\theta\,\mathrm{Cos}\,\theta)) \tag{18}$$

$$F_\theta = N(u_{r1}(\mathrm{Sin}\,\theta\,\mathrm{Cos}\,\theta) + u_{\theta 1}(\mathrm{Cos}\,\theta)^2) \tag{19}$$

Transvers field:

$$F_r = N(u_{r1}(\mathrm{Cos})^2 - u_{\theta 1}(\mathrm{Sin}\,\theta\,\mathrm{Cos}\,\theta)) \tag{20}$$

$$F_\theta = N(u_{r1}(\mathrm{Sin}\,\theta\,\mathrm{Cos}\,\theta) - u_{\theta 1}(\mathrm{Sin}\,\theta)^2) \tag{21}$$

In this study, the magnetic field has been considered with interaction parameters denoted as N_Θ ($=N$), the Lorentz force (in clear domain) is shown as:

Magnetic field around current-carrying wire:

$$F_r = -\frac{R^2 u_{r1} N}{2r^2} \tag{22}$$

$$F_\theta = 0 \tag{23}$$

Eq. (22) shows that the Lorentz force acts opposite of radial velocity (u_r) and squeezes the fluid around cylinder into the cylinder in radial direction. Note that in this case there is no Lorentz force in θ-direction. For better understanding of this effect, Fig. 4 shows the distribution of instantaneous recirculation pattern for different Stuart numbers of N = 0–0.22 with step 0.04 and N = 5, 7 and 10 at Re = 100. When N = 0 corresponding to the purely hydrodynamic case, the flow is time-dependent [19], by applying the magnetic field the radial Lorentz force (F_r) squeezes (suppresses) the fluid around the cylinder and increases the resistance for the cross flow over a cylinder. If the Stuart number increased further to 0.22, the recirculation grows up and the flow changes to the steady state and symmetric form. In range $N > 0.22$ the flow is completely steady, in this range, separation occurs earlier and separation points move upstream as the intensity of magnetic field is increased, it happened also in streamwise and transverse magnetic fields in previous studies [19] and [20]. At last, there is no vortex and flow will be similar to very low-Reynolds laminar flow.

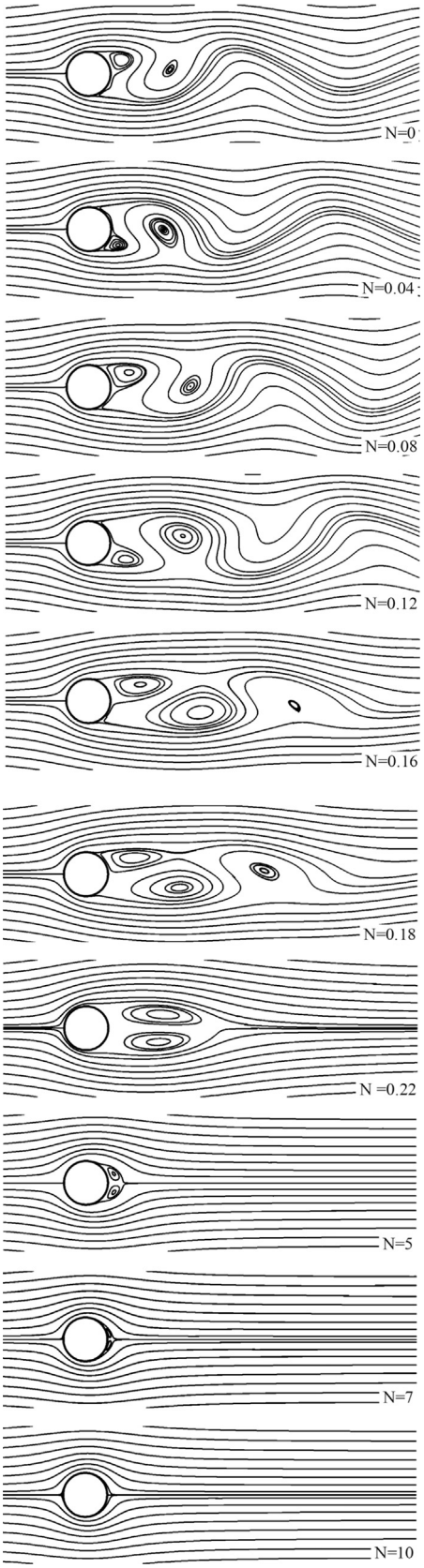

Fig.4. Instantaneous recirculation patterns for the flow over cylinder at Re = 100 with different Stuart numbers.

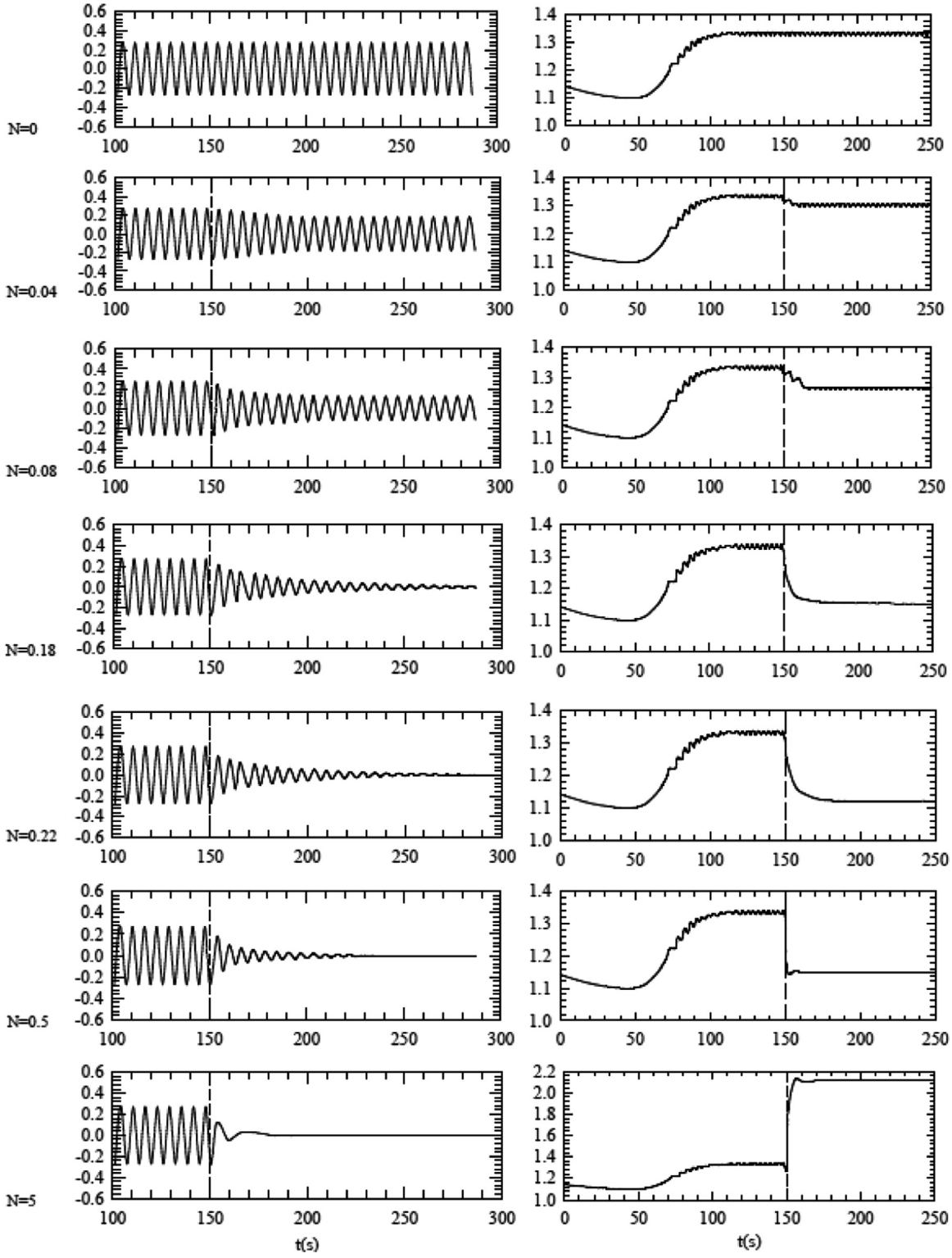

Fig. 5. Effect of the magnetic field strength on the time evolution of the lift coefficient C_L (left) and drag coefficient C_D (right) for 2-D magnetohydrodynamic flow at Re = 100 (Dashed line refer to time of applying the magnetic field).

The Lorentz force acts in radial direction and opposes the radial motion and suppresses the vortex shedding mechanism. According to the Fig. 4, at $N=10$ there is no wake and the flow will be similar to creep flow regime. In Fig. 5 for Re = 100, by applying the magnetic field at $t=150$ s the Lorentz force acts oppose the flow and by increasing "N" the lift coefficient (C_L) is reduced. It has been shown for $N=0$, 0.04, 0.08, 0.18, 0.22, 0.5 and 5 obviously. It is shown for $N<0.22$ the flow is unsteady. By applying $N=0.22$ at $t=150$ flow after about 150 seconds at $t=300$ will be steady and C_L has zero value, for $N=0.5$ it happened after 83 s. At large number of Stuart number the flow will be steady very fast, it is shown obviously for $N=5$

For the weak magnetic fields the flow remains unsteady about $N=0.21$ and at $N=0.23$ flow is completely steady, it is observed

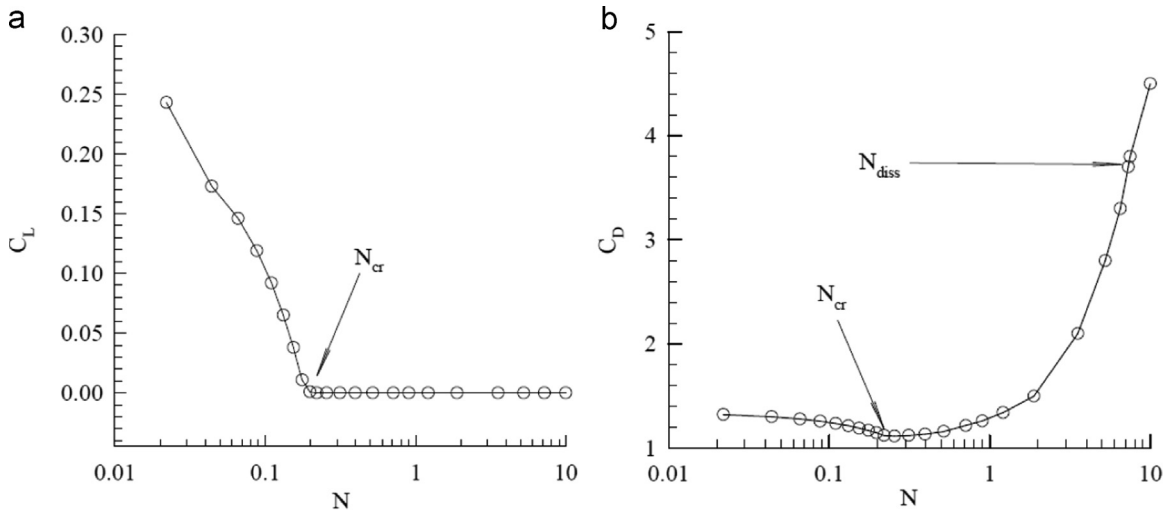

Fig. 6. (a) Lift and (b) Drag coefficients as a function of Stuart numbers for flow through a solid circular cylinder.

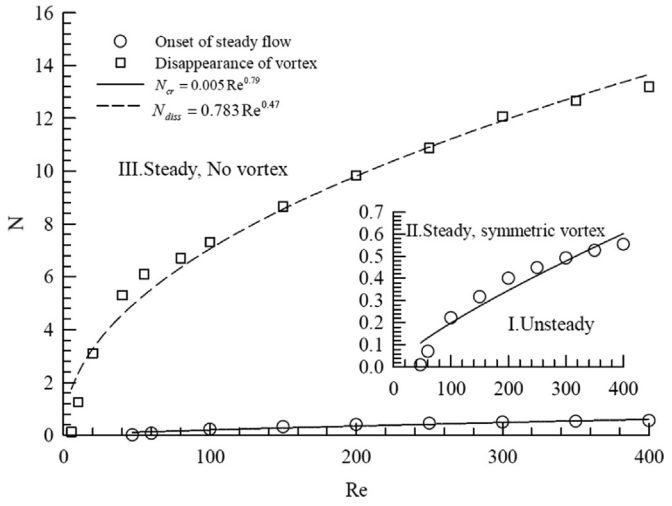

Fig. 7. The N-Re graph for separating steady and periodic flow regimes in N_{cr} and disappearing of vortex in N_{diss}.

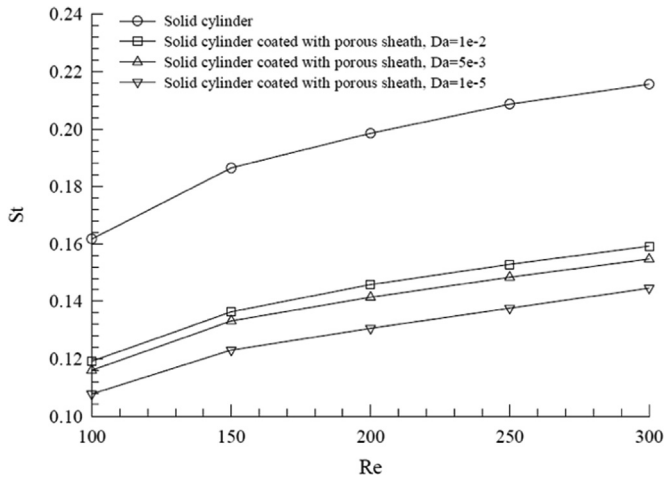

Fig. 8. Variation of St with Re for solid cylinder compared with cylinders wrapped with a porous layer.

that the critical value of interaction parameter for the transition from the unsteady regime to the steady is $N_{Cr}=0.22$, for stream-wise and transvers magnetic fields in x–y plan, the critical values at Re=100 are $N_{x,Cr}=0.15$, 0.14 and $N_{y,Cr}=0.08$, 0.1 reported in [16]

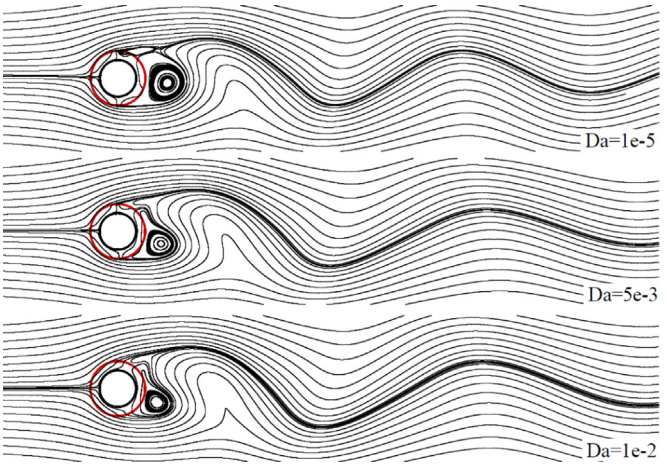

Fig. 9. Instantaneous recirculation patterns for the flow over cylinder wrapped with a porous layer at Re=100 and $N=0$ (pure hydrodynamic case).

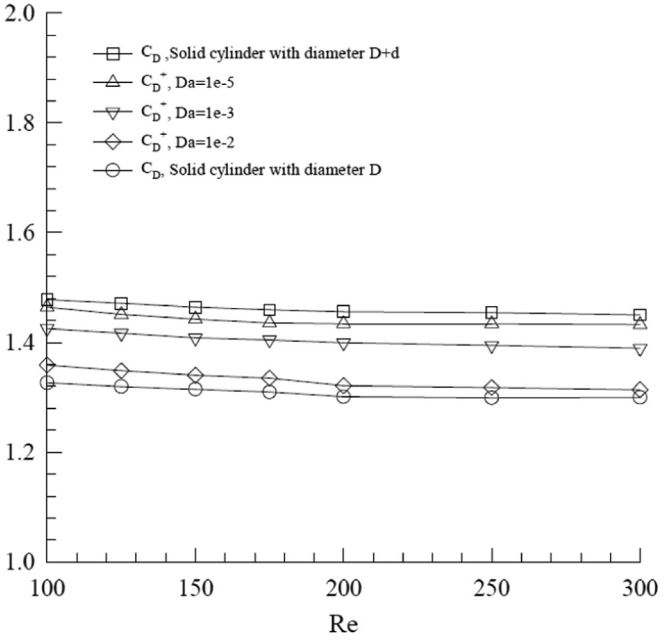

Fig. 10. Drag coefficient for purely hydrodynamic case as a function of Reynolds number for solid cylinder as compared with porous-wrapped solid cylinder.

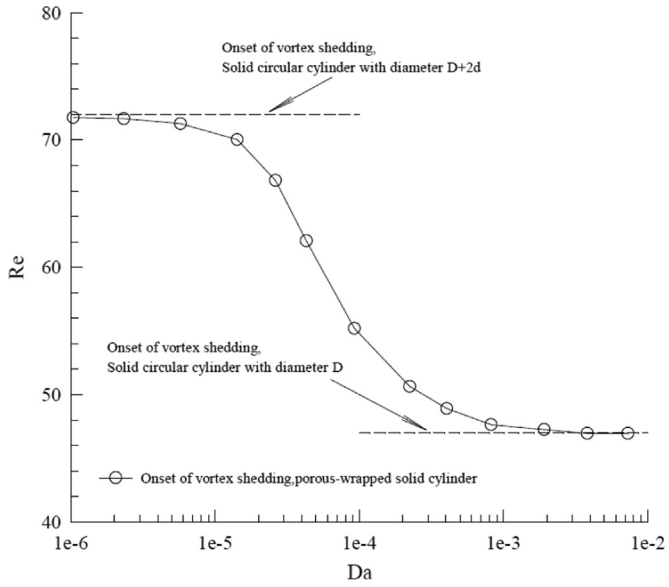

Fig. 11. The critical Reynolds number for onset of vortex shedding as a function of Da (Purly hydrodynamic case).

and [12] respectively. The effect of the magnetic field on lift and drag coefficients around solid circular cylinder can be summarized in Fig. 6(a, b). Fig. 6a shows by increasing N the lift coefficient decreases sharply and then limits to zero.

In Fig. 6b, C_D decreases slightly with increasing N until $N < N_{cr} = 0.22$. When $N = 0.22$ the C_D is the minimum value equal to 1.113 and it is 16% less than C_D value when there is no magnetic field ($N = 0$). Also by increasing $N > N_{cr} = 0.22$ C_D values increase and its value is about 3.7 when $N = N_{diss} = 7.2$ and is 63% more than C_D value in absence of magnetic field.

Fig. 7 shows the N-Re graph for magnetic field at different Re numbers. As shown in Fig. 7, the graph is divided into three regions. The critical line of transient (I) unsteady to (II) steady flow starts at Re = 48–400 and $N = 0.01$–0.55. The critical line equation can be expressed as $N_{cr} = 0.005Re^{0.79}$. This region can be named "weak magnetic field" ($N < N_{cr}$). The shear stress force decreases monotonically and thus drag coefficient decreases and has minimum value at $N = N_{cr}$ for all Re numbers 48–400. Vortex disappearance line is border between (II) steady region with symmetric vortex and (III) steady with no vortex. This line can be expressed as $N_{diss} = 0.783Re^{0.47}$. Onset of vortex for solid cylinder is at Re = 5.3 and results show by applying $N = 0.12$ vortex will disappear. The flow with Re = 400 at $N = 13.2$ the vortex will disappear. These regions (II and III) are called as "strong magnetic field regions".

6.2. For solid cylinder wrapped with a porous layer

In this section the flow field is considered for fixed value of porous layer thickness $d = 0.5R$ for range of $0 < Re < 400$. The variation in St with Re for solid cylinder with and without porous layer is shown in Fig. 8. For solid cylinder, by increasing in Re the St is increased and results show the variation of St with Re for solid cylinder wrapped with a porous layer is similar to solid one. St values for cylinder wrapped with porous layer are less than solid cylinder and a significant reduction in St values between solid cylinder and cylinder with porous layer is evident. Also increasing in Da causes to reduce in the St values due to damping effect on vortex shedding frequency.

The Instantaneous recirculation patterns for the pure hydrodynamic flow over cylinder wrapped with porous layer at Re = 100 for Da = 1e-5, 5e-3 and 1e-2 are shown in Fig. 9. Recirculation flow

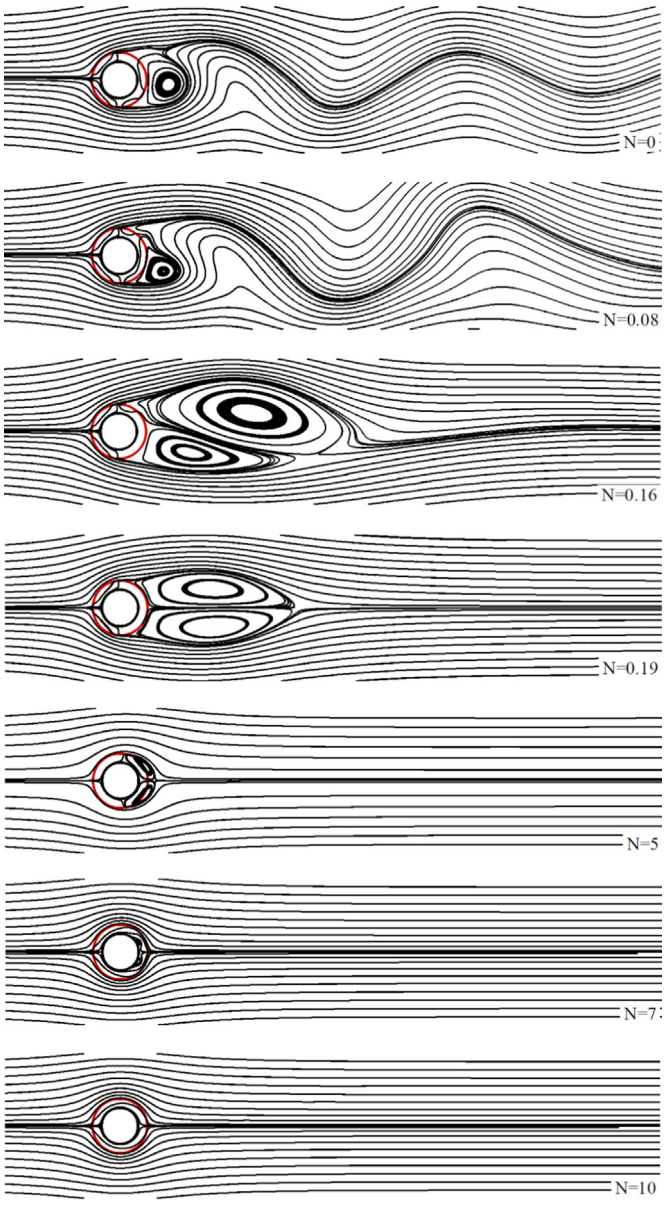

Fig. 12. Instantaneous recirculation patterns for the MHD flow over porous-wrapped solid cylinder (Da = 5e-3) at Re = 100.

behind the cylinder for Da = 1e-5 is larger than lower Da values and by increasing Da the separation point moves downstream.

Fig. 10 shows the C_D and C_D^+ values as a function of Re for solid cylinder and porous-wrapped solid cylinder. It is evident that drag increases with increase in surface area. As it is shown the C_D^+ values are less than C_D value for solid cylinder with diameter D+2d and more than C_D value for cylinder with diameter D. It can be expressed that the drag values for wrapper-porous cylinder are lower than a solid cylinder of an equal radius. For example, the C_D value of cylinder with diameter D+2d at Re = 100 is equal to 1.49, which is higher than porous-wrapped solid cylinder with same diameter and solid cylinder with diameter D.

The present simulation indicate that the Re_{cr} for solid cylinder is around 48 as shown in Fig. 11. For rigid cylinder with diameter D+2d ($d = 0.25D$) the critical Reynolds number is $72 (= 1.5 \times 48)$. For porous-wrapped solid cylinder with Da = 1e-6 the Re_{cr} is near 72. By increasing in Da from 1e-6 to 1e-2 the Re_{cr} values decrease. Re_{cr} for wrapper-porous cylinder with Da = 1e-2 is 48.3 and it is 0.3 more than rigid cylinder with diameter D.

Fig. 12 shows the Instantaneous recirculation patterns for the MHD flow over cylinder wrapped with porous layer at Re = 100 for different N and fixed Da = 5e-3. When $N = 0$ the flow is purely hydrodynamic and flow is time-dependent. If the magnetic is applied to the flow over porous-wrapped solid cylinder, the Lorentz force acts to the radial direction toward cylinder and this force increases the resistance of flow over cylinder. By increasing N further to 0.19 the flow changes to steady state and vortex shedding will be disappear. Thus the N_{cr} for porous-wrapped solid cylinder with Da = 5e-3 is 0.19 and less than its value for rigid cylinder 0.22.

7. Conclusion

The laminar flow with vortex shedding over a porous-wrapped solid cylinder in a magnetic field was investigated for Reynolds and Stuart number up to 400 and 10 respectively. The important findings of this research are listed as follows:

- The value of interaction parameter, N_{cr}, depends on the Reynolds number.
- By increasing the value of N in the range of $N < N_{cr}$, St, C_L and C_D decreases and length of recirculation increases until the flow becomes steady.
- By increasing N further in the range of $N > N_{cr}$, the flow becomes completely steady state and when apply the magnetic field C_L reaches zero value.
- The St number of porous-wrapped solid cylinder is less than that of the rigid cylinder and also when Da is decreased, St also decreases.
- The drag coefficient is higher for the porous-wrapped solid cylinder than solid cylinder in all range of Re.
- N_{cr} for porous-wrapped solid cylinder is less than the value of solid cylinder.

References

[1] A. Roshko, On the Drag and Shedding Frequency of two Dimensional Bluff Bodies, National Advisory Committee for Aeronautics (NACA), Washington, 1954, Technical Note 3169.
[2] C.H.K. Williamson, 2-D and 3-D aspects of the wake of a cylinder, and their relation to wake computations, Lect. Appl. Math. 28 (1991) 719–751.
[3] D.J. Tritton, J. Fluid Mech. 6 (1959) 547–567.
[4] L. Kun, M. Dong-jun, S. De-jun, et al., Wake patterns of flow past a pair of circular cylinders in side-by-side arrangements at low Reynolds numbers, J. Hydrodyn. Ser. B 19 (6) (2007) 690–697.
[5] M. Zhao, L. Cheng, B. Teng, D. Liang, Numerical simulation of viscous flow past two circular cylinders of different diameters, Appl. Ocean Res. 27 (1) (2005) 39–55.
[6] F. Saltara, Numerical Simulation of the Flow about Circular Cylinders (Ph.D. thesis), EPUSP University of São Paulo, Brazil (in Portuguese), 1999.
[7] K. Lee, K.S. Yang, Flow patterns past two circular cylinders in proximity, Comput. Fluids 38 (4) (2009) 778–788.
[8] J. Park, Choi K.H. Kwon, Numerical simulations of flow past a circular cylinder at Reynolds numbers up to 160, J. Mech. Sci. Technol. 12 (6) (1998) 1200–1205.
[9] S. Rashidi, J.A. Esfahani, The effect of magnetic field on instabilities of heat transfer from an obstacle in a channel, J. Magn. Magn. Mater. 391 (2015) 5–11.
[10] P.A. Davidson. An introduction to magnetohydrodynamics. Cambridge Texts in Applied Mathematics, Cambridge University press, 2001.
[11] N.B. Morley, S. Smolentsev, L. Barleon, I.R. Kirillov, M. Takahashi, Liquid magnetohydrodynamics – resent progress and future direction for fusion, Fusion Eng. Des. 51–52 (2000) 701–713.
[12] N.A. Khan, S. Aziz, N.A. Khan, MHD flow of Powell–Eyring fluid over a rotating disk, J. Taiwan Inst. Chem. Eng. 45 (2014) 2859–2867.
[13] M. Hatami, K. Hosseinzadeh, D.D. Domairry, M.T. Behnamfar, Numerical study of MHD two-phase Couette flow analysis for fluid-particle suspension between moving parallel plates, J. Taiwan Inst. Chem. Eng. 45 (2014) 2238–2245.
[14] S. Nadeem, N. Sher Akbar, Influence of heat and mass transfer on the peristaltic flow of a Johnson Segalman fluid in a vertical asymmetric channel with induced MHD, J. Taiwan Inst. Chem. Eng. 42 (2011) 58–66.
[15] G.G. Branover, Y.M. Gelfgat, S.V. Turuntaev, A.B. Tsinober, Effect of a transverse magnetic field on velocity perturbations behind a circular cylinder swept by an electrolyte, Magnetohydrodynamics (N.Y.) 7 (1) (1969) 35–41.
[16] J. Lahjomri, P. Capéran, A. Alemany, The cylinder wake in a magnetic field aligned with the velocity, J. Fluid Mech. 253 (1993) 421–448.
[17] G. Mutschke, V. Shatrov, G. Gerberth, Cylinder wake control by magnetic field in liquid metal flows, Exp. Therm. Fluid Sci. 16 (1998) 92–99.
[18] G. Mutschke, G. Gerberth, V. Shatrov, A. Tomboulides, The scenario of three-dimensional instabilities of the cylinder wake in an external magnetic field: a linear stability analysis, Phys. Fluids 13 (3) (2001) 723–734.
[19] H.S. Yoon, H.H. Chun, M.Y. Ha, H.G. Lee, A numerical study on the fluid flow and heat transfer around a circular cylinder in an aligned magnetic field, Int. J. Heat. Mass. Transf. 47 (19–20) (2004) 4075–4087.
[20] D.G.E. Grigoriadis, I.E. Sarris, S.K. Kassinos, MHD flow past a circular cylinder using immersed boundary method, Comput. Fluids 39 (2010) 345–358.
[21] S. Rashidi, M. Dehghan, R. Ellahi, M. Riaz, M.T. Jamal-Abad, Study of stream wise transverse magnetic fluid flow with heat transfer around an obstacle embedded in a porous medium, J. Magn. Magn. Mater. 378 (2015) 128–137.
[22] S. Rashidi, M. Bovand, J.A. Esfahani, H.F. Öztop, R. Masoodi, Control of wake structure behind a square cylinder by Magnetohydrodynamics, ASME J. Fluids Eng. 137 (6) (2015) 061102–061108.
[23] K.E. Kalis, A.B. Tsinober, A.G. Shtern, E.V. Shcherbinin, Flow of a conducting fluid past a circular cylinder in a transverse magnetic field, Magnetohydrodyn. (N.Y.) 1 (1) (1965) 11–19.
[24] A.B. Tsinober, P.G. Shtern, Experimental investigation of the pressure distribution forconstrained MHD flow past cylinders, Magnetohydrodyn. (N.Y.) 9 (1) (1973) 9–14.
[25] W.K. Hussam, M.C. Thompson, G.J. Sheard, Dynamics and heat transfer in a quasi-two-dimensional MHD flow past a circular cylinder in a duct at high Hartmann number, Int. J. Heat. Mass. Transf. 54 (5–6) (2011) 1091–1100.
[26] S. Rashidi, R. Masoodi, M. Bovand, M.S. Valipour, Numerical study of flow around and through a porous diamond cylinder with different apex angels. International Journal of Numerical, Methods Heat. Fluid Flow 24 (7) (2014) 1504–1518.
[27] M. Dehghan, M. Tajik Jamal-Abad, S. Rashidi, Analytical interpretation of the local thermal non-equilibrium condition of porous media imbedded in tube heat exchangers, Energy Convers. Manag. 85 (2014) 264–271.
[28] C.H. Bruneau, I. Mortazavi, Passive control of the flow around a square cylinder using porous media, Int. J. Nume. Methods Fluids 46 (2004) 415–433.
[29] C.H. Bruneau, I. Mortazavi, Control of vortex shedding around a pipe section using a porous sheath, Int. J. Offshore Polar Eng. 16 (2006) 90–96.
[30] C.H. Bruneau, I. Mortazavi, P. Gillieron, Passive control around the two-dimensional square back Ahmed body using porous devices, J. Fluids Eng. 130 (2008) 61–101.
[31] C.H. Bruneau, I. Mortazavi, Numerical modeling and passive flow control using porous media, Comput. Fluids 37 (2008) 488–498.
[32] M.P. Sobera, C.R. Kleijn, H.E.A. Van den Akker, Subcritical flow past a circular cylinder surrounded by a porous layer, Phys. Fluids 18 (2006) 38–106.
[33] P. Yu, Y. Zeng, T.S. Lee, H.X. Bai, H.T. Low, Wake structure for flow past and through a porous square cylinder, Int. J. Heat. Fluid Flow 31 (2010) 141–153.
[34] S. Rashidi, M. Bovand, I. Pop, M.S. Valipour, Numerical simulation of forced convective heat transfer past a square diamond-shaped porous cylinder, Transp. Porous Media 102 (2) (2014) 207–225.
[35] M.S. Valipour, S. Rashidi, M. Bovand, R. Masoodi, Numerical modeling of flow around and through a porous cylinder with diamond cross section. European, J. Mech. B/Fluids 46 (2014) 74–81.
[36] A.M. Abd-Alla, S.M. Abo-Dahab, R.D. Al-Simery, Effect of rotation on peristaltic flow of a micropolar fluid through a porous medium with an external magnetic field, J. Magn. Magn. Mater. 348 (2013) 33–43.
[37] C. Jiang, W. Feng, H. Zhong, J. Zeng, Q. Zhu, Effects of a magnetic quadrupole field on thermomagnetic convection of air in a porous square enclosure, J. Magn. Magn. Mater. 357 (2014) 53–60.
[38] K. Ramesh, M. Devakar, Magnetohydrodynamic peristaltic transport of couple stress fluid through porous medium in an inclined asymmetric channel with heat transfer, J. Magn. Magn. Mater. 394 (2015) 335–348.
[39] M.S. Valipour, S. Rashidi, R. Masoodi, Magnetohydrodynamics flow and heat transfer around a solid cylinder wrapped with a porous ring, ASME J. Heat Transf. 136 (2014) 062601–062609.
[40] I. Brilakis, H. Fathi, A. Rashidi, Progressive 3D reconstruction of infrastructure with videogrammetry, J. Autom. Constr. 20 (2011) 884–895.
[41] A. Rashidi, H. Fathi, I. Brilakis, Innovative stereo vision-based approach to generate dense depth map of transportation infrastructure, Transp. Res. Rec. J. Transp. Res. Board 2215 (2011) 93–99.
[42] A. Rashidi, H. Rashidi-Nejad, M. Maghiar, Productivity estimation of bulldozers using generalized linear mixed models, KSCE J. Civ. Eng. 18 (6) (2014) 1580–1589.
[43] S. Whitaker, The Forchheimer equation: a theoretical development, Transp. Porous Media 25 (1996) 27–61.
[44] S. Rashidi, A. Tamayol, M.S. Valipour, N. Shokri, Fluid flow and forced convection heat transfer around a solid cylinder wrapped with a porous ring, Int. J. Heat. Mass. Transf. 63 (2013) 91–100.
[45] M. Bovand, S. Rashidi, J.A. Esfahani, Enhancement of heat transfer by

nanofluids and orientations of the equilateral triangular obstacle, Energy Convers. Manag. 97 (2015) 212–223.
[46] A.D. Nield, A. Bejan, Convection in Porous Media, 3th edition, Springer, New York, 2006.
[47] K. Al-Salem, H.F. Oztop, S. Kiwan, Effects of porosity and thickness of porous sheets on heat transfer enhancement in a cross flow over heated cylinder, Int. Commun. Heat. Mass. Transf. 38 (2011) 1279–1282.
[48] M. Bovand, S. Rashidi, M. Dehghan, J.A. Esfahani, M.S. Valipour, Control of wake and vortex shedding behind a porous circular obstacle by exerting an external magnetic field, J. Magn. Magn. Mater. 385 (2015) 198–206.
[49] M. Dehghan, Y. Rahmani, D.D. Ganji, S. Saedodin, M.S. Valipour, S. Rashidi, Convection-radiation heat transfer in solar heat exchangers filled with a porous medium: homotopy perturbation method versus numerical analysis, Renew. Energy 74 (2015) 448–455.
[50] F.M. White, Fluid Mechanics, 6th ed., McGraw Hill Book Company, New York, 2009.
[51] S. Rashidi, M. Bovand, J.A. Esfahani, Structural optimization of nanofluid flow around an equilateral triangular obstacle, Energy (2015), http://dx.doi.org/10.1016/j.energy.2015.05.056.
[52] M.M. Zdravkovich, Flow around Circular Cylinders, Fundamentals, vol. I, Oxford Science Publications, 1997.
[53] S. Rashidi, A. Nouri-Borujerdi, M.S. Valipour, R. Ellahi, I. Pop, Stress-jump and continuity interface conditions for a cylinder embedded in a porous medium, Transp. Porous Media 107 (1) (2015) 171–186.
[54] J.A. Ochoa-Tapia, S. Whitaker, Momentum transfer at the boundary between a porous medium and a homogeneous fluid I: theoretical development, Int. J. Heat. Mass Transf. 38 (1995) 2635–2646.
[55] J.A. Ochoa-Tapia, S. Whitaker, Momentum transfer at the boundary between a porous medium and a homogeneous fluid II: comparison with experiment, Int. J. Heat. Mass. Transf. 38 (1995) 2647–2655.
[56] J.A. Ochoa-Tapia, S. Whitaker, Momentum jump condition at the boundary between a porous medium and a homogeneous fluid: inertial effect, J. Porous Media 1 (1998) 201–217.
[57] FLUENT. 6.3 User's Guide, Fluent Inc., 2006.
[58] S.V. Patankar, Numerical heat transfer and fluid flow, Hemisphere, New York, 1980.